Organic & Biomolecular Chemistry

Cite this: *Org. Biomol. Chem.*, 2012, **10**, 4577

www.rsc.org/obc

PAPER

Conformational flexibility of the pentasaccharide LNF-2 deduced from NMR spectroscopy and molecular dynamics simulations†

Elin Säwén, Florian Hinterholzinger, Clas Landersjö and Göran Widmalm*

Received 25th January 2012, Accepted 16th April 2012
DOI: 10.1039/c2ob25189b

Human milk oligosaccharides (HMOs) are important as prebiotics since they stimulate the growth of beneficial bacteria in the intestine and act as receptor analogues that can inhibit the binding of pathogens. The conformation and dynamics of the HMO Lacto-*N*-fucopentaose 2 (LNF-2), α-L-Fuc*p*-(1 → 4)-[β-D-Gal*p*-(1 → 3)]-β-D-Glc*p*NAc-(1 → 3)-β-D-Gal*p*-(1 → 4)-D-Glc*p*, having a Lewis A epitope, has been investigated employing NMR spectroscopy and molecular dynamics (MD) computer simulations. 1D ^{1}H,^{1}H-NOESY experiments were used to obtain proton–proton cross-relaxation rates from which effective distances were deduced and 2D J-HMBC and 1D long-range experiments were utilized to measure trans-glycosidic $^{3}J_{CH}$ coupling constants. The MD simulations using the PARM22/SU01 force field for carbohydrates were carried out for 600 ns with explicit water as solvent which resulted in excellent sampling for flexible glycosidic torsion angles. In addition, *in vacuo* MD simulations were performed using an MM3-2000 force field, but the agreement was less satisfactory based on an analysis of heteronuclear trans-glycosidic coupling constants. LNF-2 has a conformationally well-defined region consisting of the terminal branched part of the pentasaccharide, *i.e.*, the Lewis A epitope, and a flexible β-D-Glc*p*NAc-(1 → 3)-β-D-Gal*p*-linkage towards the lactose unit, which is situated at the reducing end. For this β-(1 → 3)-linkage a negative ψ torsion angle is favored, when experimental NMR data is combined with the MD simulation in the analysis. In addition, flexibility on a similar time scale, *i.e.*, on the order of the global overall molecular reorientation, may also be present for the ϕ torsion angle of the β-D-Gal*p*-(1 → 4)-D-Glc*p*-linkage as suggested by the simulation. It was further observed from a temperature variation study that some ^{1}H NMR chemical shifts of LNF-2 were highly sensitive and this study indicates that $\Delta\delta/\Delta T$ may be an additional tool for revealing conformational dynamics of oligosaccharides.

Introduction

Human milk oligosaccharides (HMOs) are bioactive molecules of high structural complexity[1,2] and approximately 200 individual species have been identified.[3] They are built from five different monosaccharides, *viz*., D-glucose, D-galactose, *N*-acetyl-D-glucosamine, L-fucose and sialic acid where the common scaffold is the disaccharide lactose. The milk oligosaccharide compositions vary between women and have been profiled using high-performance liquid chromatography, capillary electrophoresis and mass spectrometry techniques.[3,4] HMOs are currently being investigated for their health promoting effects and as prebiotics in the form of non-digestible compounds.[5,6] These HMOs can thus act as growth factors for beneficial *Bifidobacterium bifidum* bacteria that may colonize the colon and thus prevent the colonization by pathogenic bacteria. Furthermore, they can act as decoys thereby inhibiting attachment by bacteria, viruses and toxins.[7] There is presently a large interest in trying to emulate the HMO profiles using chemoenzymatic synthesis and biotechnology methods in order to obtain an oligosaccharide formula similar to that of natural human milk. In this respect it may be noted that bovine milk oligosaccharides are much more anionic in character with about two thirds containing either *N*-acetylneuraminic acid or *N*-glycolylneuraminic acid but fucosyl residues are absent.[8] In addition, HMOs have been shown to inhibit intestinal cell proliferation, alter cell cycle dynamics[9] and reduce HIV-1-gp120 binding to DC-SIGN.[10]

The conformation and dynamics of HMOs have been investigated using in particular NMR spectroscopy and molecular simulations.[11–15] The branched pentasaccharide Lacto-*N*-fucopentaose 2 (LNF-2), α-L-Fuc*p*-(1 → 4)[β-D-Gal*p*-(1 → 3)]-β-D-Glc*p*NAc-(1 → 3)-β-D-Gal*p*-(1 → 4)-α-D-Glc*p*, derivatives thereof and the Lewis A trisaccharide, α-L-Fuc*p*-(1 → 4)[β-D-Gal*p*-(1 → 3)-D-Glc*p*NAc, which corresponds to the terminal part of LNF-2 were studied with respect to overall three-dimensional structure and

Department of Organic Chemistry, Arrhenius Laboratory, Stockholm University, S-106 91 Stockholm, Sweden. E-mail: gw@organ.su.se
† Presented in part at the 238th ACS National Meeting, Washington, DC, United States, August 16–20, 2009.

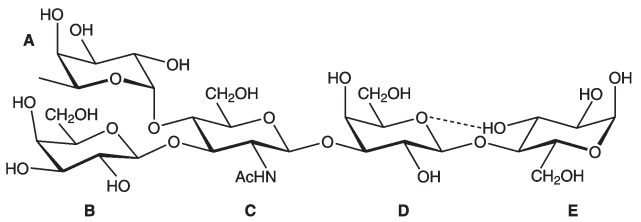

Fig. 1 Schematic of the pentasaccharide lacto-*N*-fucopentaose 2 (LNF-2), α-L-Fuc*p*-(1 → 4)[β-D-Gal*p*-(1 → 3)]-β-D-Glc*p*NAc-(1 → 3)-β-D-Gal*p*-(1 → 4)-α-D-Glc*p* with sugar residues labeled A–E, respectively. A hydrogen bond present in the MD simulations with explicit water between O5 in D and HO3 in E is denoted by a dashed line.

flexibility in different parts of the molecule.[16–23] We herein analyze the conformational preferences and dynamics of LNF-2 (Fig. 1) using experimental ^{1}H,^{1}H-NOE and $^3J_{CH}$ data combined with molecular dynamics (MD) simulations.

Materials and methods

General

Lacto-*N*-fucopentaose 2 was obtained from IsoSep AB (Tullinge, Sweden). The torsion angles in LNF-2 across the glycosidic linkages are defined as follows: ϕ_A = H1A-C1A-O4C-C4C, ψ_A = C1A-O4C-C4C-H4C, according to the nomenclature in Fig. 1 and so on. Associated with the ψ_C torsion angle, C1C-O3D-C3D-H3D, the two conformational states are referred to as $\psi_C^+ > 0°$ and $\psi_C^- < 0°$. For the Boltzmann constant k_B a value of 0.00198721 kcal mol^{-1} K^{-1} was used.

NMR spectroscopy

NMR experiments were carried out at 315 K and a concentration of 60 mM (Shigemi tube BMS-005TV, Shigemi, Allison Park, PA, USA) in D_2O containing 20 mM phosphate buffer (pD_c = 7.1) on 600 and 800 MHz Varian Inova spectrometers equipped with 5 mm PFG triple-resonance probes and in 5 mm tubes at 280 and 315 K with a concentration of 42 mM in D_2O on Bruker Avance 500 MHz and Avance III 700 MHz spectrometers equipped with 5 mm cryoprobes.

For proton and carbon chemical shift assignments of LNF-2 at 315 K ^{1}H,^{13}C-HSQC, ^{1}H,^{1}H-HSQC-TOCSY (mixing times of 40 and 80 ms), ^{1}H,^{1}H-TOCSY (mixing times of 10, 30, 60, 90 and 120 ms) and ^{1}H,^{13}C-H2BC experiments were used. Spectra were referenced to internal sodium 3-trimethylsilyl-(2,2,3,3-$^2H_4$)-propanoate (TSP, δ_H 0.00). Carbon-13 NMR chemical shifts were referenced to external 1,4-dioxane in D_2O (δ_C 67.40). Measurements of the temperature dependence on the ^{1}H NMR chemical shifts were performed with 1D experiments at ten different temperatures ranging from 281–357 K.

Measurements of the trans-glycosidic carbon–proton coupling constants were performed with Hadamard excitations of the selected ^{13}C resonances as described previously[24,25] and with the ^{1}H,^{13}C-J-HMBC experiment.[26] In the J-HMBC experiments different values of the scaling factor, κ = 13.7, 20.6 and 24.5, were used to scale splitting of the doublet components in the indirect dimension. Spectral widths of 10 ppm for ^{1}H and 60–100 ppm for ^{13}C were used. The experiments were performed with 3072 × 512 points and 32–48 scans per t_1 increment with the echo/antiecho method. Forward linear prediction to 1024 points in the F_1-dimension, subsequent zero-filling to 4096 × 16 384 points and a 90° shifted squared sine-bell function were applied prior to Fourier transformation. The J-HMBC spectrum was processed in magnitude mode. Coupling constants were extracted from 1D-projections of the resonances of interest.

Proton–proton cross-relaxation rates in LNF-2 were obtained at 315 K at a ^{1}H frequency of 800 MHz employing 2D ^{1}H,^{1}H-NOESY experiments[27] and at 280 K at a ^{1}H frequency of 700 MHz using 1D DPFGSE ^{1}H,^{1}H-NOESY experiments.[28] For the 1D experiments selective excitations of H1A, H5A, H1B and H4D were enabled using 50 Hz broad r-Snob-2 shaped pulses. For each excited resonance five different mixing times ranging from 120–360 ms were used; a relaxation delay of >5 × T_1 was used in all cases. The isolated spin-pair approximation (ISPA)[29] was used to compare the cross-relaxation rate of the reference spin pair, σ_{ref} to that of protons i and j, denoted σ_{ij}. Subsequently, the unknown distance, r_{ij}, between the protons was obtained according to $r_{ij} = r_{ref}(\sigma_{ref}/\sigma_{ij})^{1/6}$.

Computer simulations

Based on the knowledge that there may be more than a single low energy conformation at each glycosidic linkage in HMOs,[11] such a structure was chosen as the initial conformation of LNF-2. Four sets of MD simulations were performed, one in vacuum and three in explicit water. For the molecular dynamics (MD) simulations in explicit water, CHARMM (parallel version, C34b2) software[30] was used employing a CHARMM22 type of force field[31] modified for carbohydrates and referred to as PARM22/SU01.[32] Initial conditions were prepared by placing the pentasaccharide in a previously equilibrated cubic water box of length 40.39 Å containing 2197 modified TIP3P water molecules.[33] The solvent molecules that were closer than 2.5 Å to any solute atom were removed resulting in 2130 TIP3P water molecules. After heating and equilibration, two production runs were performed at 315 K for 200 ns each and one production run was performed at 280 K for 200 ns. The MD simulations in vacuum were performed using the "Dynamic Molecules" webservice[34] using the TINKER31 (version 4.2) suite (http://dasher.wustl.edu/tinker, accessed July 2008) and employing an MM3-2000 force field. The simulations were performed in vacuum at 315 K for various times ranging from 2 ns to 200 ns with a time step of 1 ps. The dielectric constant was set to a value of ε = 4.30.

Results and discussion

NMR spectroscopy

The ^{1}H and ^{13}C NMR chemical shifts of LNF-2 have previously been assigned at different temperatures[35–38] and were herein assigned at 315 K (Table 1). For the conformational studies proton–proton cross-relaxation rates from ^{1}H,^{1}H-NOESY experiments and trans-glycosidic heteronuclear coupling constants

Table 1 ^{1}H and ^{13}C NMR chemical shifts (ppm) of LNF-2 at 42 °C; internal TSP and external 1,4-dioxane in D_2O was used as references, respectively

Residue		1	2	3	4	5	6
α-L-Fuc*p*-(1 → 4)	A	5.03	3.81	3.89	3.80	4.85	1.19
		98.82	68.68	70.01	72.79	67.60	16.18
β-D-Gal*p*-(1 → 3)	B	4.52	3.49	3.63	3.90	3.57	3.74, 3.74
		103.58	71.40	73.25	69.18	75.65	62.39
→3,4)-β-D-Glc*p*NAc-(1 →	C	4.74	3.95	4.10	3.76	3.56	3.87, 3.95
		103.29	56.73	76.82	73.09	76.13	60.58
→3)-β-D-Gal*p*-(1 → [a,b]	D	4.451	3.60	3.72	4.16	3.72	3.75, 3.79
		103.76	70.83	82.88	69.12	75.70	61.75
→4)-β-D-Glc*p*	E_β	4.67	3.29	3.65	3.65	3.60	3.80, 3.95
		96.57	74.67	75.21	79.32	70.81	61.01
→4)-α-D-Glc*p*	E_α	5.23	3.59	3.84	3.64	3.95	3.84, 3.89
		92.66	72.01	72.23	79.41	70.96	60.90

[a] NMR chemical shift for NAc are δ_H 2.04; δ_C 23.16 and 175.55. [b] NMR chemical shifts for anomeric atoms in D when residue E has the α-configuration: δ_{H1} 4.452 and δ_{C1} 103.72.

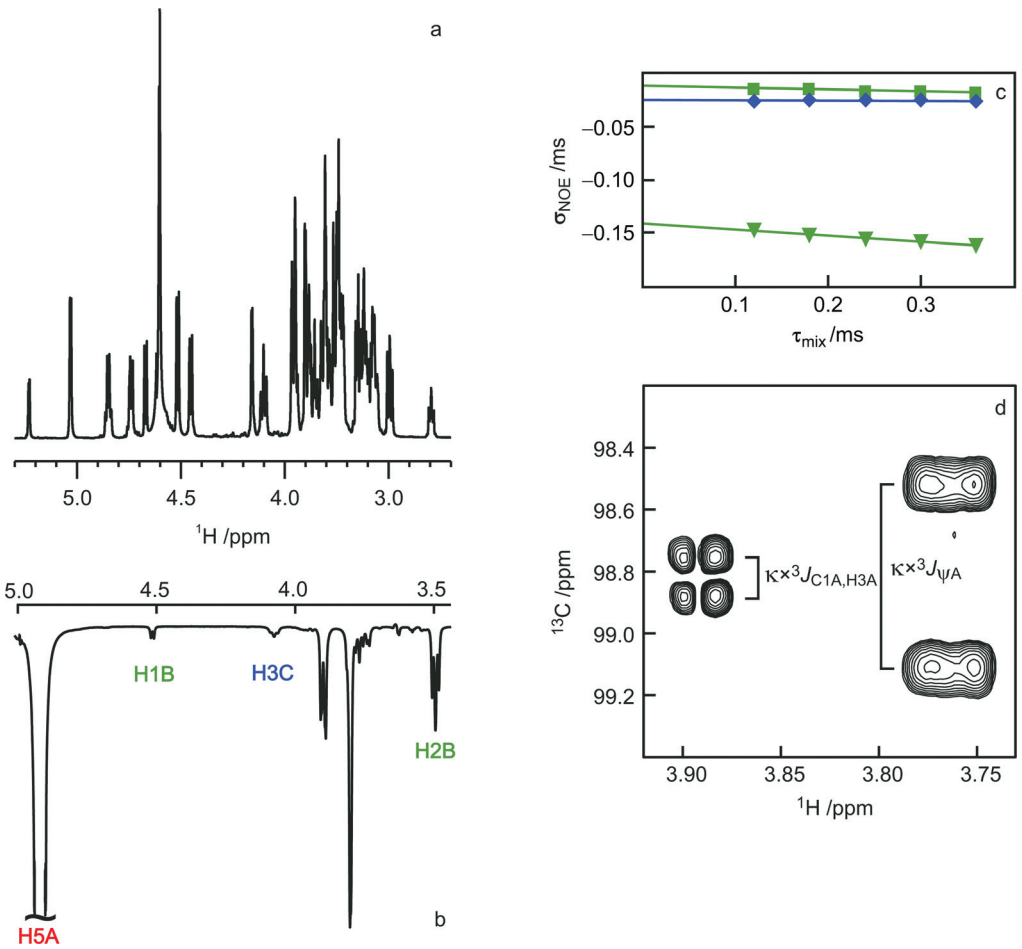

Fig. 2 (a) Selected spectral region of a ^{1}H NMR spectrum of LNF-2; (b) 1D $^{1}H,^{1}H$-DPFGSE-NOESY spectrum of LNF-2 recorded at 280 K on a 700 MHz spectrometer with selective excitation of H5A and a mixing time of 180 ms; (c) plot of $-I_j(\tau_{mix})/[\tau_{mix}I_i]$ *versus* τ_{mix}, where I_j is the intensity of the NOE-peak and I_i is the intensity of the target peak, showing the inter-residue cross-relaxation rates (obtained from the extrapolation to the ordinate) from H1B (green squares), H3C (blue diamonds), and H2B (green triangles); (d) selected spectral region of a J-HMBC spectrum where the experiment was recorded at 315 K; the apparent splitting of the doublet components by $\kappa \times {}^{3}J_{CH}$ in the indirect dimension was achieved with a scaling factor $\kappa = 20.6$ and the cross-peak separations are related to the trans-glycosidic torsion angle ψ_A ($^{3}J_{C1A,H4C} = 5.0$ Hz) and the intra-residue correlation between C1A and H3A ($^{3}J_{C1A,H3A} = 1.1$ Hz).

were acquired. The $^{1}H,^{1}H$-NOESY experiments were carried out first at 315 K using the two-dimensional variant at a ^{1}H frequency of 800 MHz. Several NOE build-up curves[27] were of high precision, but analysis of consistency for intra-residue

correlations (with known effective distances from MD simulations, *vide infra*) revealed that the accuracy from the 2D experiment was in general lower than needed. One conclusion was, however, drawn from the experiment, *viz.*, that the effective trans-glycosidic distance between H1 in residue C and H3 in residue D was short, <2.3 Å, which is consistent with a conformational study of), α-L-Fuc*p*-(1 → 4)-β-D-Glc*p*NAc-(1 → 3)-β-D-Gal*p*-OMe,[39] corresponding to the entity A-C-D in LNF-2. Subsequently, we turned to one-dimensional ^{1}H,^{1}H-NOESY experiments using selective excitations of a specific proton having a well-resolved resonance in the ^{1}H NMR spectrum (Fig. 2a). Since the ^{1}H frequency was now 700 MHz we lowered the temperature to 280 K, in order to obtain sufficiently large and negative NOEs. An example of this is shown in Fig. 2b, in which important detectable NOEs are present from H5A to H1B, H2B and H3C. From the NOE build-up curves analyzed as described,[40,41] intra- and inter-residue cross-relaxation rates were obtained as the intercepts with the ordinate (Fig. 2c) and are compiled in Table 2. Utilizing an intra-residue reference distance from MD simulations (*vide infra*) effective proton–proton distances were subsequently obtained.

Trans-glycosidic heteronuclear coupling constants were determined using a 1DLR experiment[24,25] from which in this case only two values could be extracted with confidence (Table 3). The two-dimensional J-HMBC experiment[26] was successfully employed (Fig. 2d) in order to obtain seven out of the eight $^{3}J_{CH}$ couplings (Table 3). The last one, $^{3}J_{C1D,H4E}$, which is related to the reducing end residue being an α/β-anomeric mixture was not possible to obtain with sufficient confidence. The experimental uncertainty is for the first technique on the order of 0.2 Hz[42] and for the second one about 0.25 Hz.[26] Thus, the acquired coupling constants using two independent NMR experiments for each one of the correlations $^{3}J_{C1A,H4C}$ and $^{3}J_{H1B,H3C}$ are the same, within experimental error, with one large coupling of ~5 Hz and one of intermediate magnitude, being ~3 Hz, respectively. The standard deviations in $^{3}J_{CH}$ from the J-HMBC experiment were for some of the values on the order of the estimated uncertainty of the technique but in most cases significantly lower. The previously reported $^{3}J_{CH}$ data on LNF-2 using the q-HMQC experiment[38] (Table 3) both agree and disagree (difference >0.5 Hz) with the present data.

We now have two types of experimental data, effective proton–proton distances from NOE data and trans-glycosidic coupling constants that conformationally can be interpreted *via* Karplus-type relationships, and for the subsequent analysis we rely on molecular models generated by MD simulations presented below.

Table 2 Inter- and intra-residue cross-relaxation rates for LNF-2 from 1D H,^{1}H-NOESY experiments at a proton frequency of 700 MHz and a temperature of at 280 K, experimentally derived distances r_{expt} and calculated r_{calc} distances from the MD simulation with explicit water

Proton pair	σ_{NOE}/s^{-1}	r_{expt}/Å	r_{calc}/Å
H1A–H4C	−0.239	2.33	2.42
H5A–H2B	−0.140	2.54	2.52
H5A–H3C	−0.0243	3.41	3.63
H1B–H5A	−0.0109[a]	3.93	3.92
H1B–H2B	−0.0491	3.04	3.05
H1B–H3B	−0.167	2.47[b]	2.47
H1B–H3C	−0.185	2.43	2.42
H4D–H1C	−0.0396	3.14	3.46

[a] Averaged value from excitation of both resonances in the proton pair. [b] Intra-residue reference distance from MD simulation.

MD simulations

Two types of simulations were performed, *viz.*, of LNF-2 *in vacuo*, since the approach facilitates rapid computations of accessible conformational space,[43] and with explicit water as solvent since it should lead to a more appropriate description of the solute molecule and its interactions with the solvent. In the first case MD simulations were performed ranging from 2 ns to 200 ns using an MM3-2000 force field and comparisons to experimental NMR data indicated that conformational sampling during 200 ns was sufficient under the simulation protocol used. The conformational space populated for the glycosidic linkages is shown by scatter plots in Fig. 3, from which it can be deduced that the flexibility is quite large. In the second case the MD simulations were carried out twice with a 200 ns duration staring from a conformationally accessible region[22] with different seeds for initial velocities. In this case the PARM22/SU01 force field was used with explicit water molecules as solvent. During the first two ns of simulation transitions occurred from a ϕ_A^-/ψ_A^- state to a ϕ_A^+/ψ_A^+ state which then remained as the sole

Table 3 Averages from the MD simulations of LNF-2 in vacuum (200 ns) and in explicit water (400 ns) together with the torsion angle span observed by XRD for the Lewis A trisaccharide bound to PA-IIL. Experimental $^{3}J_{CH}$ coupling constants for LNF-2 averaged from five different J-HMBC experiments with varying κ, from 1DLR measurements and compared to literature data (q-HMQC).

Torsion angle	MD_v/°	MD_w/°	Lewis A/°	Coupling constant	Experiment			MD simulation	
					J-HMBC/Hz	1DLR/Hz	q-HMQC/Hz	J_v/Hz	J_w/Hz
ϕ_A	10 [25][a]	38 [19]	43–53	$J_{\phi A}$	2.84 [0.03]			4.6	4.0
ψ_A	−38 [102]	21 [15]	15–19	$J_{\psi A}$	4.97 [0.07]	5.0		4.5	5.1
ϕ_B	19 [15]	47 [10]	42–58	$J_{\phi B}$	2.86 [0.22]	3.2	2.7	4.8	3.6
ψ_B	34 [12]	17 [9]	9–24	$J_{\psi B}$	4.97 [0.21]		5.7	4.2	5.6
ϕ_C	29 [16]	47 [13]	n.a.[b]	$J_{\phi C}$	4.19 [0.06]			4.0	3.6
ψ_C	−36 [36]	7 [37]	n.a.	$J_{\psi C}$	4.62 [0.04]		4.0	3.1	4.1
ϕ_D	38 [13]	43 [19]	n.a.	$J_{\phi D}$	4.01 [0.06]		3.1	3.3	3.6
ψ_D	−13 [19]	1 [18]	n.a.	$J_{\psi D}$			3.2	5.4	5.7

[a] Standard deviations in square brackets. [b] n.a. = not applicable.

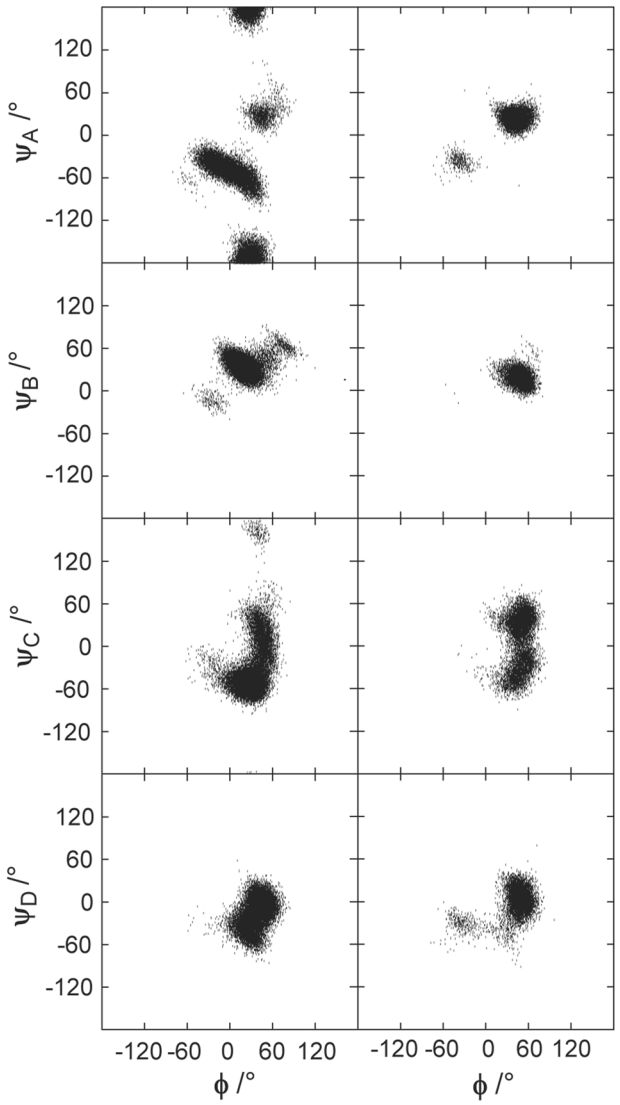

Fig. 3 Scatter plots of ψ *vs.* ϕ, for the four different glycosidic linkages in LNF-2 from the 200 ns long MD simulation in vacuum at 315 K (left column) and the 400 ns long MD simulation in explicit water at 315 K (right column).

conformational state for the α-L-Fuc*p*-(1 → 4)-β-D-Glc*p*NAc-linkage up to the finish of the two simulations at 200 ns. In the simulations with explicit water the conformational space was overall less sampled although the flexibility was still significant for the β-D-Glc*p*NAc-(1 → 3)-β-D-Gal*p*-linkage (Fig. 3). The glycosidic torsion angles and their standard deviations are compiled in Table 3 for the two types of MD simulations.

The probability distributions were then analyzed for the MD simulation with explicit water molecules (disregarding the initial ϕ_A^-/ψ_A^- state) and for the α-L-Fuc*p*-(1 → 4)-β-D-Glc*p*NAc-linkage and the β-D-Gal*p*-(1 → 3)-β-D-Glc*p*NAc-linkage of the terminal trisaccharide part of the pentasaccharide making up a Lewis A epitope the distributions are narrow (Fig. 4) and the trisaccharide can be described by a single conformational state. The conformations of the Lewis A trisaccharide when bound to the PA-IIL lectin[44] exhibit a small span (Table 3) and the conformational preferences for the glycosidic torsions from the simulation with explicit water are within this span for the β-(1 → 3)-linkage or very close to it (within one standard deviation) for the α-(1 → 4)-linkage, whereas for the *in vacuo* simulations deviations are larger or very large. With respect to the β-D-Glc*p*NAc-(1 → 3)-β-D-Gal*p*-linkage two significantly populated states are present at the ψ_C torsion angle (Fig. 4g) consistent with MD simulations performed with an OPLS-AA force field and the SPC water model.[22] For the β-D-Gal*p*-(1 → 4)-D-Glc*p*-linkage it is instead the ϕ_D torsion angle which shows the presence of a small population of a non-*exo*-anomeric conformation in addition to the major anticipated *exo*-anomeric conformation (Fig. 4d).

The free energy for the latter two torsion angles were obtained by calculating the potential of mean force (PMF) over the MD simulation according to $W(\phi) = -k_BT \ln p(\phi)$, where $p(\phi)$ is the probability distribution obtained from the MD simulation; the distribution for the torsion angle ψ was generated in an equivalent way. For the ψ_C torsion angle of the β-(1 → 3)-linkage the free energy difference between the ψ_C^+ and ψ_C^- states is small, only 0.5 *kT* (Fig. 5a). The free energy difference between the ϕ_D^+ and ϕ_D^- states of the β-(1 → 4)-linkage is larger, about 2 *kT* (Fig. 5b). Identifying the presence of two interconverting conformational states then facilitated the investigation of the relaxation process jumping between two wells by calculating a number correlation function $C_N(t)$ where each state along a trajectory was identified as unity if the molecule has the conformation of the reactant well and zero if it is in the product well.[45] The relaxation time τ_N for the process was determined by fitting the decay (Fig. 6) to a mono-exponential function and resulted in similar time scales for the two processes, *viz.*, ~170 ps related to the ψ_C torsion angle and ~190 ps related to the ϕ_D torsion angle. The relaxation time τ_N for the interconverting process at the β-(1 → 3)-linkage is slower in LNF-2 than in LNF-1 where it was found to be ~100 ps[46] using the same force field. However, it is still anticipated to occur on the same time scale as the overall reorientation of the whole molecule.

Intra-molecular hydrogen bonding was also analyzed from the MD simulations using geometric criteria, *viz.*, a hydrogen bond is present if the distance between the hydrogen atom and the acceptor atom is <2.5 Å with the donor-hydrogen-acceptor angle > 135°, and the one between O5D and HO3E (Fig. 1) was significant with an occurrence of 43%. This indicates that hydrogen bonding would be of importance in stabilizing the major conformational state, but its detection in methyl α-cellobioside which has the same geometric arrangements at the β-(1 → 4)-linkage has been elusive.[47]

In this section we obtained dynamical models by MD simulations and these may now be used in the further analysis where experimental data are taken into consideration in order to generate a conformational description of LNF-2 in solution.

Experiment *vs.* simulation

From the MD simulation of LNF-2 in water at 280 K effective proton–proton distances were calculated according to $1/r_{calc} = \langle r^{-6} \rangle^{1/6}$ (Table 2). Using H1B–H3B as a reference distance experimentally determined distances were obtained by applying ISPA (*vide supra*) and these results are also shown in Table 2.

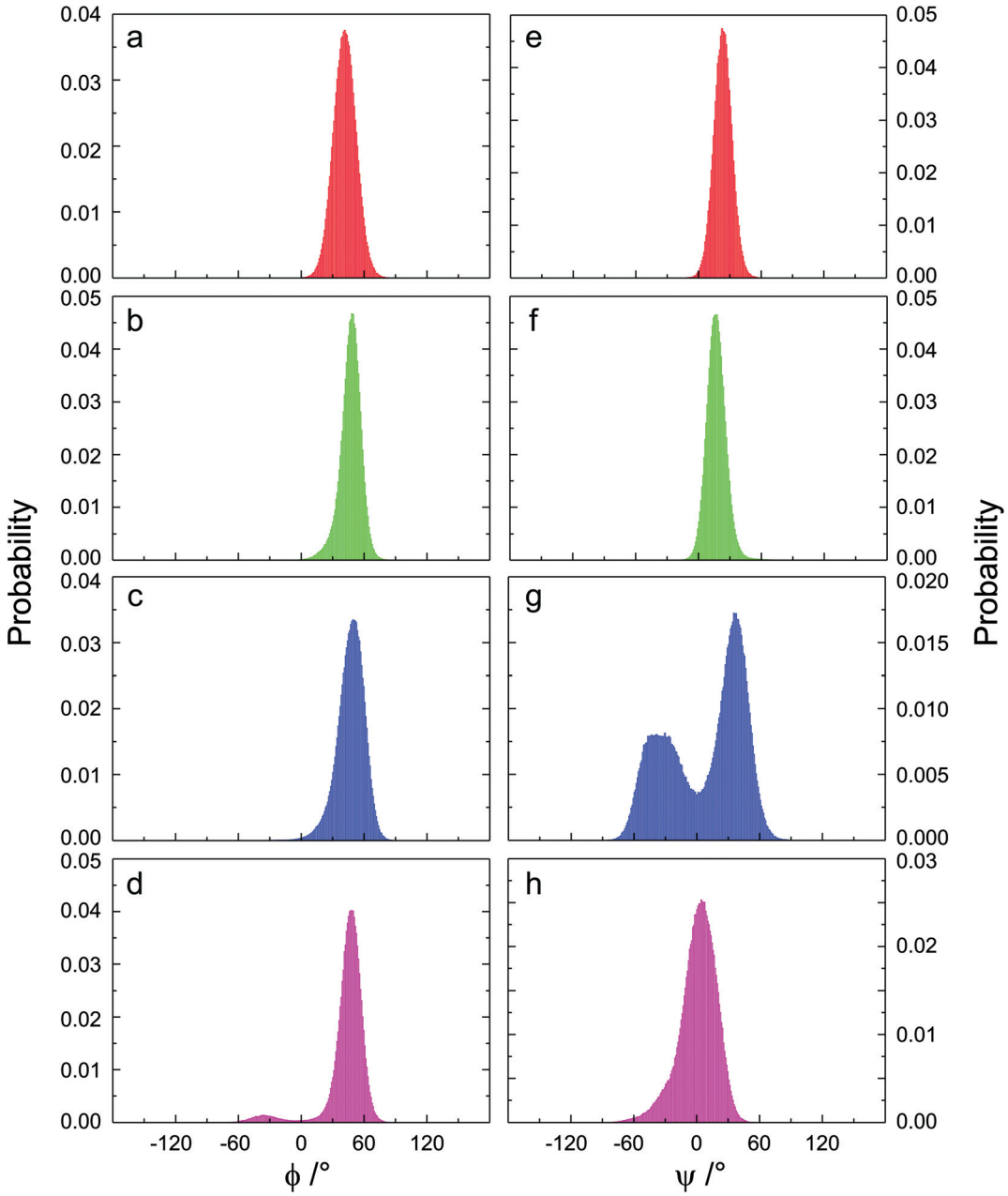

Fig. 4 Probability distributions of the glycosidic torsion angles from the MD simulations at 315 K with explicit water molecules (except for the first few ns where a ϕ_A^-/ψ_A^- state was populated) using a bin size of 1°; (a) and (e) show the torsion angles between residues A and C, (b) and (f) between residues B and C, (c) and (g) between residues C and D and (d) and (h) the torsion angles between residues D and E.

When determining the H1B–H2B distance within the same sugar ring the experimental and calculated distances are in accord, lending credence to the 1D NOE methodology used. In the terminal trisaccharide part of the molecule the agreement between experimentally observed effective proton–proton distances and those calculated by the MD simulation was very good (Table 2) supporting the proposed relatively rigid structure of the Lewis A epitope, in agreement with previous studies on this structural entity.[18,21,36] For the challenging inter-residue distances very good agreement is again seen, including also the H1C–H3D distance being 2.42 Å in the simulation and somewhat shorter from NMR experiment (*vide supra*). Of the determined distances the largest deviation between experiment and simulation was present for the H1C–H4D distance, *i.e.*, the distance which is sensitive to the ψ_C conformational distribution, as previously shown for LNF-1 and LNnT.[46,48] The experimentally determined short distance of 3.14 Å in LNF-2 supports the ψ_C^- conformational state as the major one and ψ_C^+ as the minor one, in contrast to the equilibrium proposed from the present MD simulation which favors the latter. The combined results describing LNF-2 with ψ_C^- as the preferred conformational state is in accord with previous studies on this pentasaccharide.[19,20,23]

From the MD simulations *in vacuo* and in water trans-glycosidic $^3J_{CH}$ coupling constants were calculated for LNF-2 using the

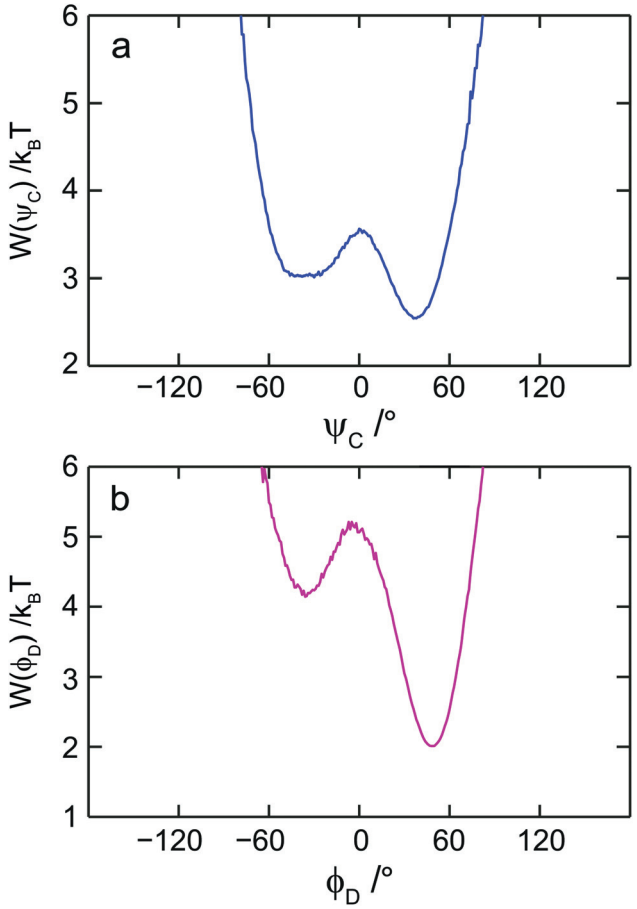

Fig. 5 Potential of Mean Force (PMF) of the glycosidic torsion angles ψ_C (a) and ϕ_D (b) from the 400 ns MD simulation at 315 K.

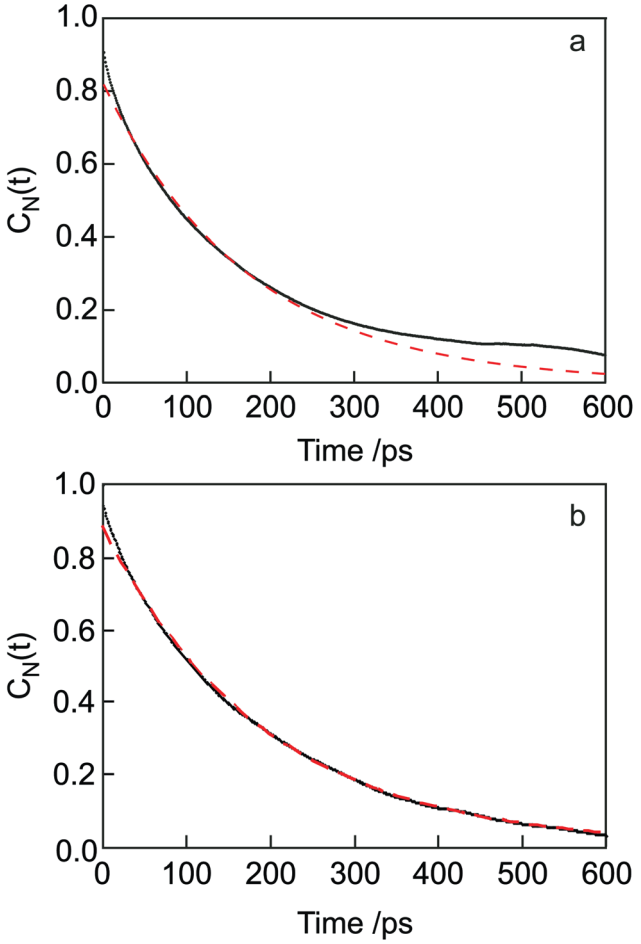

Fig. 6 Number correlation function $C_N(t)$ for the isomerization process at the glycosidic torsion angles ψ_C (a) and ϕ_D (b) from the 400 ns simulation. The red dashed line shows a mono-exponential decay obtained from the fit to $C_N(t)$ between 10–260 ps, τ_N = 171 ps for ψ_C and τ_N = 192 ps for ϕ_D.

recently developed Karplus-type relationships for oligosaccharides denoted JCX/SU09.[49] The agreement between the experimentally determined trans-glycosidic $^3J_{CH}$ coupling constants and those calculated from the simulations were ascertained by defining a residual factor R_J:

$$R_J = N^{-1} \sum_{i=1}^{N} (|J_i^{expt} - J_i^{calc}|/|J_i^{expt}|) \quad (1)$$

where J_i^{expt} is the ith experimentally determined $^3J_{CH}$ coupling constant and J_i^{calc} is the corresponding coupling constant calculated from the MD simulations and N is the number of observations (*i.e.*, the number of coupling constants included in the analysis). The R_J value from the *in vacuo* simulation was 0.30 whereas from the in water simulation it was lower, being 0.17. These results support the glycosidic torsion angle conformational distributions from the MD simulation with explicit water as the preferred ones and show that the distributions from the *in vacuo* simulation agree less well with experimental $^3J_{CH}$ data. A comparison between the heteronuclear coupling constants determined by the J-HMBC experiment and those calculated based on the MD simulations with explicit water as solvent (Table 3, Fig. 7) reveal that the conformational preferences of the ϕ and ψ glycosidic torsion angles are captured by the PARM22/SU01 force field in which $J_\phi < J_\psi$, further supporting the proposed 3D structure of the pentasaccharide.

^{1}H chemical shift *vs.* temperature

In the present study we began by assigning ^{1}H and ^{13}C NMR chemical shifts of LNF-2 at 315 K. The continued analysis herein at the lower temperature of 280 K highlighted that some chemical shifts did change a good deal with temperature whereas other did not. We therefore carried out a temperature variation study on LNF-2 between 8 and 84 °C. Whereas *e.g.* H1A and H1B did not show any chemical shift displacement, H5A and H1C did with negative and positive slopes of similar magnitude, respectively (Fig. 8). From the present study H1C was shown to be present at a glycosidic linkage where flexibility between two states occurs and the $\Delta\delta/\Delta T$ may be an indication of this. Even though H1A is insensitive to the temperature increase, an upfield ^{1}H chemical shift displacement takes place for H5A and could indicate that a second conformational region is accessed to some extent at the higher temperature in LNF-2, which is a branched

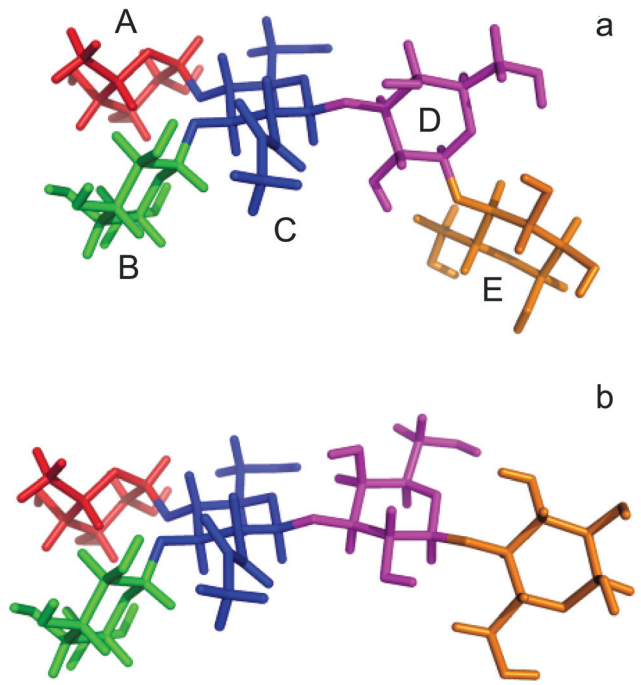

Fig. 7 Molecular models of LNF-2 from the MD simulation in explicit water at 315 K with average values for the glycosidic torsion angles. For the β-(1 → 3)-linkage between residues C and D both conformational states are shown with (a) $\langle\psi_C^+\rangle = 35°$ and (b) $\langle\psi_C^-\rangle = -34°$.

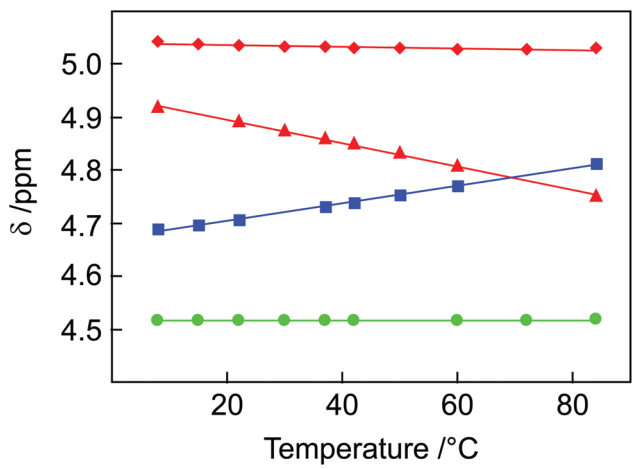

Fig. 8 Plot of ^{1}H chemical shifts *vs.* temperature; variation of the temperature was performed between 8 and 84 °C. The proton chemical shift dependency on the temperature is shown for H1A (red diamonds), H5A (red triangles), H1C (blue squares) and H1B (green circles). For H5A $\Delta\delta/\Delta T = -2.2$ ppb K^{-1} and for H1C $\Delta\delta/\Delta T = 1.7$ ppb K^{-1}.

pentasaccharide. This is possibly the ϕ_A^-/ψ_A^- state, which has been shown to be accessible on the Ramachandran potential energy surface.[22] A similar upfield ^{1}H chemical shift displacement occurs for H5 in a rhamnosyl residue which is present in the backbone of a polysaccharide that has branched tetrasaccharide repeating units.[50] A detailed investigation of the temperature dependence would require, *e.g.*, MD simulations at several temperatures, which is outside the scope of this study, but the presented results indicate that temperature variation studies may shed additional light on the conformational flexibility of oligosaccharides and could be useful for other systems.

Conclusions

The conformational analysis of the LNF-2 pentasaccharide reveals a molecule which has both a well-defined region and a flexible region. The Lewis A trisaccharide can thus be treated as an entity connected to lactose, in between which flexibility occurs at a ψ torsion angle. Additional flexibility can be anticipated within the lactose entity to some extent. For LNF-2 the intrinsic flexibility is suggested to be present on a time scale similar to that of the overall global reorientation of the molecule. The very small free energy difference between the ψ_C^+ and ψ_C^- states of the β-D-Gal*p*-(1 → 3)-β-D-Glc*p*NAc-linkage from the MD simulations highlights the difficulties of molecular mechanics force fields to predict the exact potential energy surface for a molecule. However, since the present force fields are of good quality any minor discrepancies may be handled by an approach that also relies on experimental data, as was the case in the present investigation. The major conformer could then be determined as the ψ_C^- state, but a conformational equilibrium between two states at this glycosidic linkage is still a suitable description (Fig. 7). From a biological point of view we note that the bioactive LNF-2 pentasaccharide, with its Lewis A epitope, may have a prearranged three-dimensional structure for binding to the *Pseudomonas aeruginosa* PA-IIL lectin.[44] LNF-2 is a HMO of very high potency to this protein[51] and we speculate that an additional function of this pentasaccharide is to protect the infant from such an opportunistic pathogen.

Acknowledgements

This work was supported by grants from the Swedish Research Council and The Knut and Alice Wallenberg Foundation. Computing resources were kindly provided by the Center for Parallel Computers (PDC), Stockholm, Sweden.

Notes and references

1 W. Chai, V. E. Piskarev, Y. Zhang, A. M. Lawson and H. Kogelberg, *Arch. Biochem. Biophys.*, 2005, **434**, 116–127.
2 S. Wu, N. Tao, J. B. German, R. Grimm and C. B. Lebrilla, *J. Proteome Res.*, 2010, **9**, 4138–4151.
3 M. R. Ninonuevo, Y. Park, H. Yin, J. Zhang, R. E. Ward, B. H. Clowers, J. B. German, L. S. Freeman, K. Killeen, R. Grimm and C. B. Lebrilla, *J. Agric. Food Chem.*, 2006, **54**, 7471–7480.
4 R. Mehra and P. Kelly, *Int. Dairy J.*, 2006, **16**, 1334–1340.
5 C. Kunz and S. Rudloff, *Int. Dairy J.*, 2006, **16**, 1341–1346.
6 D. A. Sela and D. A. Mills, *Trends Microbiol.*, 2010, **18**, 298–307.
7 R. M. Espinosa, M. Taméz and P. Prieto, *Br. J. Nutr.*, 2007, **98**, S74–S79.
8 N. Tao, E. J. DePeters, J. B. German, R. Grimm and C. B. Lebrilla, *J. Dairy Sci.*, 2009, **92**, 2991–3001.
9 S. Kuntz, C. Kunz and S. Rudloff, *Br. J. Nutr.*, 2009, **101**, 1306–1315.
10 P. Hong, M. R. Ninonuevo, B. Lee, C. Lebrilla and L. Bode, *Br. J. Nutr.*, 2009, **101**, 482–486.
11 G. Widmalm and R. M. Venable, *Biopolymers*, 1994, **34**, 1079–1088.
12 T. Rundlöf, C. Landersjö, K. Lycknert, A. Maliniak and G. Widmalm, *Magn. Reson. Chem.*, 1998, **36**, 773–776.
13 T. Rundlöf, R. M. Venable, R. W. Pastor, J. Kowalewski and G. Widmalm, *J. Am. Chem. Soc.*, 1999, **121**, 11847–11854.

14 A. Almond, B. O. Petersen and J. Ø. Duus, *Biochemistry*, 2004, **43**, 5853–5863.
15 S. Ganguly, J. Xia, C. Margulis, L. Stanwyck and C. A. Bush, *Biopolymers*, 2011, **95**, 39–50.
16 B. Bechtel, A. J. Wand, K. Wroblewski, H. Koprowski and J. Thurin, *J. Biol. Chem.*, 1990, **265**, 2028–2037.
17 H. Kogelberg and T. J. Rutherford, *Glycobiology*, 1994, **4**, 49–57.
18 H. Kogelberg, T. A. Frenkiel, S. W. Homans, A. Lubineau and T. Feizi, *Biochemistry*, 1996, **35**, 1954–1964.
19 M. Martin-Pastor and C. A. Bush, *Carbohydr. Res.*, 2000, **323**, 147–155.
20 M. Manuel-Pastor and C. A. Bush, *Biochemistry*, 2000, **39**, 4674–4683.
21 H. F. Azurmendi, M. Martin-Pastor and C. A. Bush, *Biopolymers*, 2002, **63**, 89–98.
22 J. Xia and C. Margulis, *J. Biomol. NMR*, 2008, **42**, 241–256.
23 J. Xia, C. Margulis and D. A. Case, *J. Am. Chem. Soc.*, 2011, **133**, 15252–15255.
24 T. Nishida, G. Widmalm and P. Sándor, *Magn. Reson. Chem.*, 1996, **34**, 377–382.
25 T. Rundlöf, A. Kjellberg, C. Damberg, T. Nishida and G. Widmalm, *Magn. Reson. Chem.*, 1998, **36**, 839–847.
26 A. Meissner and O. W. Sørensen, *Magn. Reson. Chem.*, 2001, **39**, 49–52.
27 G. Widmalm, R. A. Byrd and W. Egan, *Carbohydr. Res.*, 1992, **229**, 195–211.
28 K. Stott, J. Keeler, Q. N. Van and A. J. Shaka, *J. Magn. Reson.*, 1997, **125**, 302–324.
29 P. D. Thomas, V. J. Basus and T. L. James, *Proc. Natl. Acad. Sci. U. S. A.*, 1991, **88**, 1237–1241.
30 B. R. Brooks, R. E. Bruccoleri, B. D. Olafson, D. J. States, S. Swaminathan and M. Karplus, *J. Comput. Chem.*, 1983, **4**, 187–217.
31 A. D. MacKerell Jr., D. Bashford, M. Bellott, R. L. Dunbrack Jr., J. D. Evanseck, M. J. Field, S. Fischer, J. Gao, H. Guo, S. Ha, D. Joseph-McCarthy, L. Kushnir, K. Kuczera, F. T. K. Lau, C. Mattos, S. Michnick, T. Ngo, T. D. Nguyen, B. W. E. Reiher III, B. Roux, M. Schlenkrich, J. C. Smith, R. Stote, J. Straub, M. Watanabe, J. Wiórkiewicz-Kuczera, D. Yin and M. Karplus, *J. Phys. Chem. B*, 1998, **102**, 3586–3616.
32 R. Eklund and G. Widmalm, *Carbohydr. Res.*, 2003, **338**, 393–398.
33 E. Neria, S. Fischer and M. Karplus, *J. Chem. Phys.*, 1996, **105**, 1902–1921.
34 M. Frank, P. Gutbrod, C. Hassayoun and C.-W. von der Lieth, *J. Mol. Model.*, 2003, **9**, 308–315.
35 J. Breg, D. Romijn, J. F. G. Vliegenthart, G. Strecker and J. Montreuil, *Carbohydr. Res.*, 1988, **183**, 19–34.
36 P. Cagas and C. A. Bush, *Biopolymers*, 1990, **30**, 1123–1138.
37 K. Hermansson, P.-E. Jansson, L. Kenne, G. Widmalm and F. Lindh, *Carbohydr. Res.*, 1992, **235**, 69–81.
38 Q. Xu, R. Gitti and C. A. Bush, *Glycobiology*, 1996, **6**, 281–288.
39 T. Jackson, V. Robertson, A. Imberty and F.-I. Auzanneau, *Bioorg. Med. Chem.*, 2009, **17**, 1514–1526.
40 A. M. Dixon, G. Widmalm and T. E. Bull, *J. Magn. Reson.*, 2000, **147**, 266–272.
41 K. H. M. Jonsson, R. Pendrill and G. Widmalm, *Magn. Reson. Chem.*, 2011, **49**, 117–124.
42 T. Nishida, G. Widmalm and P. Sandor, *Magn. Reson. Chem.*, 1995, **33**, 596–599.
43 I. Sánchez-Medina, M. Frank, C.-W. von der Lieth and J. P. Kamerling, *Org. Biomol. Chem.*, 2009, **7**, 280–287.
44 S. Perret, C. Sabin, C. Dumon, M. Pokorná, C. Gautier, O. Galanina, S. Ilia, N. Bovin, M. Nicaise, M. Desmadril, N. Gilboa-Garber, M. Wimmerová, E. P. Mitchell and A. Imberty, *Biochem. J.*, 2005, **389**, 325–332.
45 R. W. Pastor, in *The Molecular Dynamics of Liquid Crystals*, ed. G. R. Luckhurst and C. A. Veracini, Kluwer, Dordrecht, 1994, pp. 85–138.
46 E. Säwén, B. Stevensson, J. Östervall, A. Maliniak and G. Widmalm, *J. Phys. Chem. B*, 2011, **115**, 7109–7121.
47 W. Zhang, H. Zhao, I. Carmichael and A. S. Serianni, *Carbohydr. Res.*, 2009, **344**, 1582–1587.
48 C. Landersjö, J. L. M. Jansson, A. Maliniak and G. Widmalm, *J. Phys. Chem. B*, 2005, **109**, 17320–17326.
49 E. Säwén, T. Massad, C. Landersjö, P. Damberg and G. Widmalm, *Org. Biomol. Chem.*, 2010, **8**, 3684–3695.
50 E. Säwén, J. Östervall, C. Landersjö, M. Edblad, A. Weintraub, M. Ansaruzzaman and G. Widmalm, *Carbohydr. Res.*, 2012, **348**, 99–103.
51 A. M. Wu, J. H. Wu, T. Singh, J.-H. Liu, M.-S. Tsai and N. Gilboa-Garber, *Biochimie*, 2006, **88**, 1479–1492.